Acta Metall. Sin. (Engl. Lett.), 2016, **29**(6), 577–586
DOI 10.1007/s40195-016-0423-0

Hydrogen Storage Thermodynamics and Dynamics of Nd–Mg–Ni-Based $NdMg_{12}$-Type Alloys Synthesized by Mechanical Milling

Yang-Huan Zhang[1,2] · Ze-Ming Yuan[2] · Wen-Gang Bu[2] · Feng Hu[1,2] · Ying Cai[1] · Dong-Liang Zhao[2]

Received: 25 December 2015 / Revised: 31 March 2016 / Published online: 3 May 2016

Abstract Nanocrystalline and amorphous $NdMg_{12}$-type $NdMg_{11}Ni + x$ wt% Ni ($x = 100$, 200) hydrogen storage alloys were synthesized by mechanical milling. The effects of Ni content and milling time on hydrogen storage thermodynamics and dynamics of the alloys were systematically investigated. The gaseous hydrogen absorption and desorption properties were investigated by Sieverts apparatus and differential scanning calorimeter connected with a H_2 detector. Results show that increasing Ni content significantly improves hydrogen absorption and desorption kinetics of the alloys. Furthermore, varying milling time has an obvious effect on the hydrogen storage properties of the alloys. Hydrogen absorption saturation ratio (R^{a}_{10}; a ratio of the hydrogen absorption capacity in 10 min to the saturated hydrogen absorption capacity) of the alloys obtains the maximum value with varying milling time. Hydrogen desorption ratio (R^{d}_{20}, a ratio of the hydrogen desorption capacity in 20 min to the saturated hydrogen absorption capacity) of the alloys always increases with extending milling time. The improved hydrogen desorption kinetics of the alloys are considered to be ascribed to the decreased hydrogen desorption activation energy caused by increasing Ni content and milling time.

KEY WORDS: $NdMg_{12}$ alloy; Hydrogen storage; Mechanical milling; Activation energy; Kinetics

1 Introduction

Intensive efforts have been made for developing and promoting the wide application of fuel cell vehicles to effectively control the increasingly serious environmental pollution, and intemperate use of fossil fuels resulted from transport [1]. A key technical challenge for the realization of onboard fuel cell or hydrogen-fueled vehicles is to develop a practical hydrogen storage system [2]. Among hydrogen storage methods, hydrogen storage in metal hydrides is considered to be one of the most promising alternatives to meet the requirements for mobile application [3, 4]. Several hydrogen storage materials have been reported for achieving the application goal, but none of them can meet all the performance requirements proposed by US Department of Energy (DOE) for vehicular applications [5, 6]. In consideration of irreplaceable advantages, Mg-based alloys are considered to be a leading candidate for hydrogen fuel cell vehicles. Especially, the Mg-rich rare earth Mg-based alloy has attracted increasing interest due to its gaseous hydrogen storage capacity of 3.7–6.0 wt% [7] and the theoretical electrochemical capacity of over 1000 mAh/g [8], much higher than those of Mg–Ni alloy. However, some inherent issues of the Mg-based alloys, such as relatively high hydrogen desorption temperature, sluggish hydriding/dehydriding kinetics and extremely low electrochemical discharge capacity at room temperature, severely hinder their

Available online at http://link.springer.com/journal/40195

✉ Yang-Huan Zhang
zhangyh59@sina.com

[1] Key Laboratory of Integrated Exploitation of Baiyun Obo Multi-Metal Resources, Inner Mongolia University of Science and Technology, Baotou 014010, China

[2] Department of Functional Material Research, Central Iron and Steel Research Institute, Beijing 100081, China

practical application as the hydrogen storage materials of onboard use or as the negative electrode materials of Ni–MH batteries. Facing such huge difficulties, researchers around the world have been unceasingly devoting themselves to realizing the application target.

Summarization in numerous publications regarding the upgrade of hydrogenation properties of Mg-based alloys finds that primary principles for improving the hydrogen storage properties of Mg-based alloys are no more than two categories: The first one is to prepare an ultra-fine microstructure and reduce the grain size far below the micrometer scale [9], and the second one is to add catalytic elements such as transition metals, transition metal oxides and rare earth (RE) metals [10–12]. Some techniques, including mechanical milling [13], rapid solidification [14], hydriding combustion synthesis [15] and equal channel angular pressing [16], have been successfully applied to the preparations of the amorphous and nanocrystalline Mg-based alloys with different compositions. Mechanical milling and melt spinning, in particular, are universally accepted techniques for obtaining amorphous and/or nanocrystalline alloys with a very homogeneous element distribution. Wang et al. [17] investigated the electrochemical hydrogen storage properties of ball-milled $MmMg_{12}$ alloy with Ni powder and found that the first discharge capacity of the ball-milled sample was enhanced from 770 to 1200 mAh/g by increasing Ni content in the alloy from 150 to 200 wt%. Yartys et al. [18] reported that the $LaMg_{11}Ni$ alloy solidified at the highest cooling rate exhibited the fastest hydrogenation kinetics, reaching the maximum hydrogenation capacity of 5.02 wt%. Zhang et al. [19] reported that the as-spun $Mg_{10}NiR$ (R = La, Nd and Sm) alloys exhibited superior hydriding and dehydriding kinetics as a result of adding different rare earth elements.

Thus, the hydrogen sorption properties of Mg-based alloys can be significantly enhanced by adding Ni and ball milling treatment. Therefore, Mg in the $NdMg_{12}$-type alloy was partially substituted by Ni in the present work. Nanocrystalline and amorphous $NdMg_{11}Ni + x$ wt% Ni (x = 100, 200) alloys were prepared by mechanical milling, and the effects of Ni content and milling time on the hydrogen storage performance of the alloys have been investigated in detail.

2 Experimental

The $NdMg_{11}Ni$ alloy was prepared by using a vacuum induction furnace in a helium atmosphere at a pressure of 0.04 MPa to prevent Mg from volatilizing. The molten alloy was poured into a cooled copper mold, and then a cast ingot was obtained. The as-cast alloys were mechanically crushed into powder with a diameter of approximately 50 μm. The alloy powder is mixed with carbonyl nickel powder at weight ratios of 1:1 and 1:2, respectively. Then, the mixed powder was mechanically milled in a planetary-type mill and handled in a glove box under an Ar atmosphere to prevent the powder from oxidation during ball milling. Cr–Ni stainless steel ball and the powder with a weight ratio of 35:1 were put into Cr–Ni stainless steel vials together. Milling speed was 135 rpm, and duration time was 5, 10, 20, 40 and 60 h, respectively. For simplicity, the chemical composition of ball-milled alloys was defined as $NdMg_{11}Ni + x$ wt% Ni (x = 100, 200), and all the hydrogen absorption and desorption capacities of the samples were calculated based on $NdMg_{11}Ni$ (excluding the mass of carbonyl nickel powder during ball milling).

The phase structures of the as-cast and milled alloys were determined by X-ray diffraction (XRD, D/max/2400), using CuK_{α} radiation filtered by graphite at 160 mA, 40 kV and 10°/min. A Philips scanning electron microscope (SEM, Quanta 400) linked with an energy-dispersive spectrometer (EDS) was used for observing morphologies and analyzing chemical compositions of the as-cast alloys. The powder samples of the as-milled alloys were observed by high resolution transmission electron microscope (HRTEM, JEM-2100F, operated at 200 kV), and their crystalline states were ascertained by electron diffraction (ED).

The hydrogen absorption and desorption kinetics and pressure–composition isotherms (P–C–T) of the alloys were measured by using an automatically controlled Sieverts apparatus with a furnace controlled to an accuracy of ±2 K. Prior to measurement, several hydrogen absorption and desorption cycles were performed to activate the materials. An initial hydrogen pressure of 3 MPa was applied to induce hydrogen absorption of the alloy particles at the temperatures of 553, 573, 593 and 613 K as well as hydrogen desorption at a pressure of 1×10^{-4} MPa at the same temperatures. 300 mg sample was loaded into a cylindrical reactor for each measurement. Hydrogen desorption properties were also measured by using a differential scanning calorimeter (DSC, SDT Q600) at the heating rates of 5, 10, 15 and 20 K/min.

3 Results and Discussion

3.1 Microstructure Characteristics

The phase components and structure characteristics of the as-cast and milled $NdMg_{11}Ni + x$ wt% Ni (x = 0, 100, 200) alloys before and after hydriding are subjected to XRD analysis, just as shown in Fig. 1. The phase identifications were carried out by using MDI Jade6.0 software.

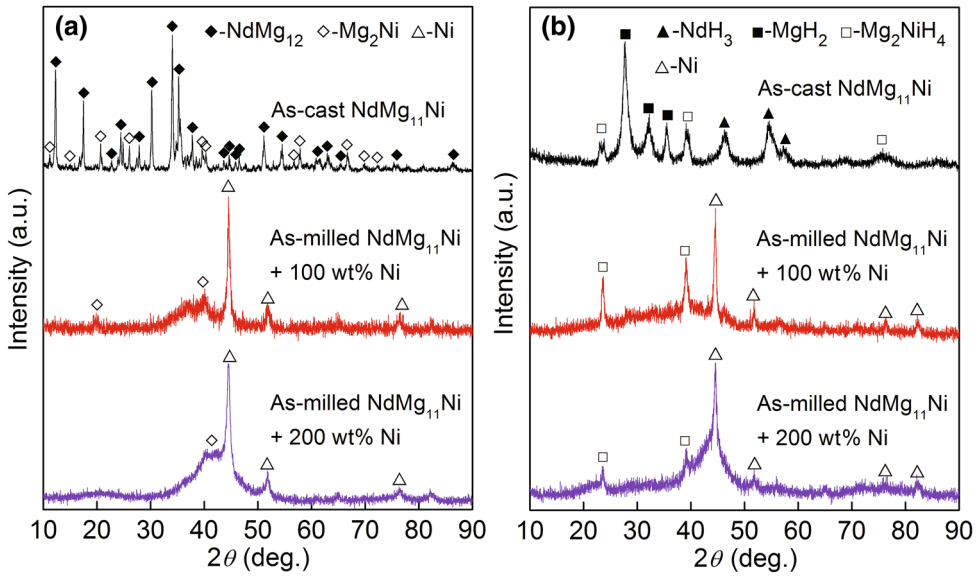

Fig. 1 XRD profiles of the as-cast and milled (10 h) $NdMg_{11}Ni + x$ wt% Ni ($x = 0$, 100, 200) alloys before and after hydriding. **a** Before, **b** after hydriding

It has been experimentally determined that the as-cast $NdMg_{11}Ni$ alloy usually has structures with a major phase $NdMg_{12}$ and a secondary phase Mg_2Ni. The abundances of the $NdMg_{12}$ and Mg_2Ni phases are calculated to be 91 wt% ($NdMg_{12}$) and 9 wt% (Mg_2Ni) according to the XRD pattern. The mechanical milling results in the diffraction peaks merging and dramatic broadening, leaving only the excess Ni. This is ascribed to the remarkable refinement of the alloy grains and the formation of an Mg_2Ni-type amorphous structure during ball milling. The strong Ni diffraction peaks in the ball-milled alloy are mainly because Ni has better toughness, and it is difficult to transform into amorphous structure. Also, the broadened degree of the diffraction peaks of the alloys obviously increases with growing Ni content, suggesting that increasing Ni content facilitates the glass forming of the alloy, which is evidenced by Abdellaoui et al. [20]. It can be found from Fig. 1b that there are three hydrides occurring in the hydriding process of the as-cast alloy, including NdH_3, MgH_2 and Mg_2NiH_4, which result from the following reactions [21, 22]: $NdMg_{12} + H_2 \rightarrow MgH_2 + NdH_3$, $Mg_2Ni + H_2 \rightarrow Mg_2NiH_4$. Besides, it is noted that after hydriding, the diffraction peaks of the alloys clearly broaden, which is most likely attributed to the lattice expansion in the process of hydrogen absorption. The as-milled $NdMg_{11}Ni + x$ wt% Ni ($x = 100$, 200) alloys in a saturated hydrogen absorption state still display nanocrystalline and amorphous structures, implying that the as-milled alloys have a good structure stability.

Figure 2 presents the SEM images and EDS patterns of the as-cast $NdMg_{11}Ni$ alloy, which exhibits a typical casting morphology. And different structure shapes can be clearly observed in the pictures. Among them, the block shape in the dark gray color is ascertained to be the major phase $NdMg_{12}$. The other displays a net-like morphology in the dark gray color distributing on the major phase, and the amplified morphology is found to have a black-and-white-like sandwich structure. The EDS profiles reveal that the dark gray zone is the $NdMg_{12}$ phase, and the gray zone is the Mg_2Ni phase.

HRTEM micrographs and ED patterns of the as-milled $NdMg_{11}Ni + x$ wt% Ni ($x = 100$, 200) alloys are demonstrated in Fig. 3. We note that the alloy particles obviously agglomerate together though dispersed strongly in alcohol. And it is found from Fig. 3c, d that the mechanical milling makes the crystalline alloy strongly disordered and nanostructured. Also, some crystal defects, such as dislocation, grain boundary and twin, can be clearly observed in the as-milled alloys. The lattice spaces of the phases are directly measured according to the HRTEM image, and then indexed them to the different phases based on the standard crystalline interplanar spacing in PDF cards.

3.2 *P–C–T* Curves and Thermodynamics

Figure 4 shows the *P–C–T* curves of the as-milled $NdMg_{11}Ni + x$ wt% Ni ($x = 100$, 200) alloys at 573 K. It is found that the absorption and desorption pressure plateaus of the as-milled alloys exhibit a clear inclination and

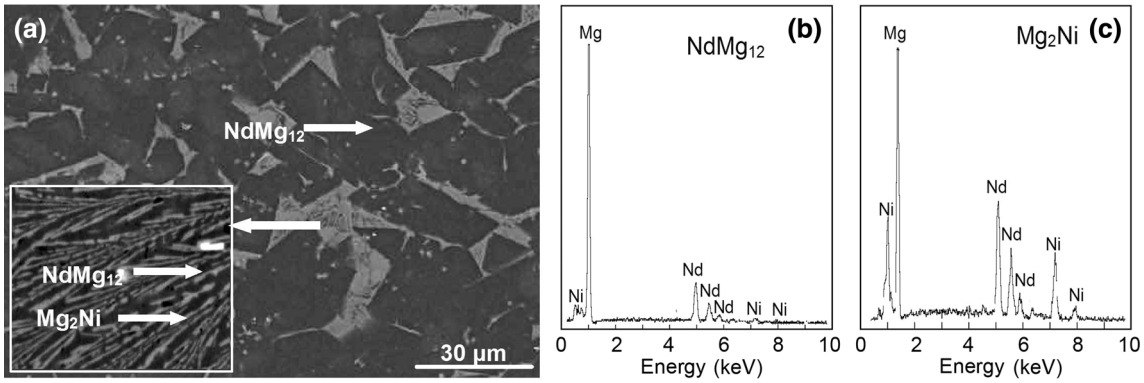

Fig. 2 SEM images **a** together with typical EDS spectra **b**, **c** of the as-cast $NdMg_{11}Ni$ alloy

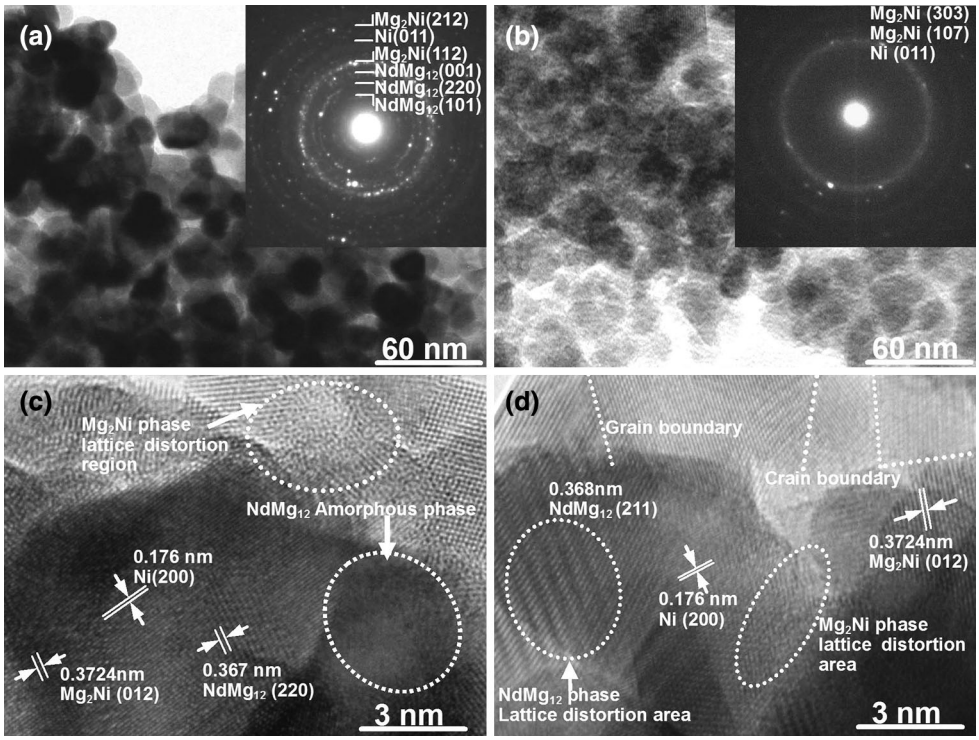

Fig. 3 HRTEM micrographs and ED patterns of the as-milled (10 h) $NdMg_{11}Ni + x$ wt% Ni ($x = 100$, 200) alloys. **a**, **c** $x = 100$, **b**, **d** $x = 200$

a large hysteresis ($H_f = \ln(P_a/P_d)$). And the pressure plateaus of the alloys visibly raise with increasing milling time, suggesting that varying milling time could also affect the hydrogen desorption thermodynamic behavior of the alloys. Moreover, we also note that milling time has an evident effect on the hydrogen storage capacity of the alloys. The variations of the hydrogen storage capacities of the alloys with milling time are shown in the inset of Fig. 4. It is evident to see that the hydrogen storage capacities of the alloys first augment and then decline with prolonged milling time, and the maximum values are 5.813 and 6.112 wt% for the ($x = 100$, 200) alloys, respectively, indicating that increasing Ni content gives rise to a positive action on the hydrogen absorption capacity of the as-milled alloys. To examine the gaseous hydrogen absorption/desorption thermodynamics of as-milled $NdMg_{11}Ni + x$ wt% Ni ($x = 100$, 200) alloys, the *P–C–T* curves of the alloys were measured at 553, 573, 593 and 613 K, respectively, as illustrated in Fig. 5. Based on Fig. 5, Van't Hoff diagrams for the hydrogen absorption/desorption of the alloys can be plotted, as shown in the inset of Fig. 5. It is worth noting that there are good linear relations between $\ln P_{H_2}/P_0$ and $1/T$ for the $NdMg_{11}Ni + x$ wt% Ni ($x = 100$, 200) alloys. Thus, the thermodynamic parameters, namely enthalpy ΔH and entropy ΔS, can be easily calculated from Van't Hoff equation [23]:

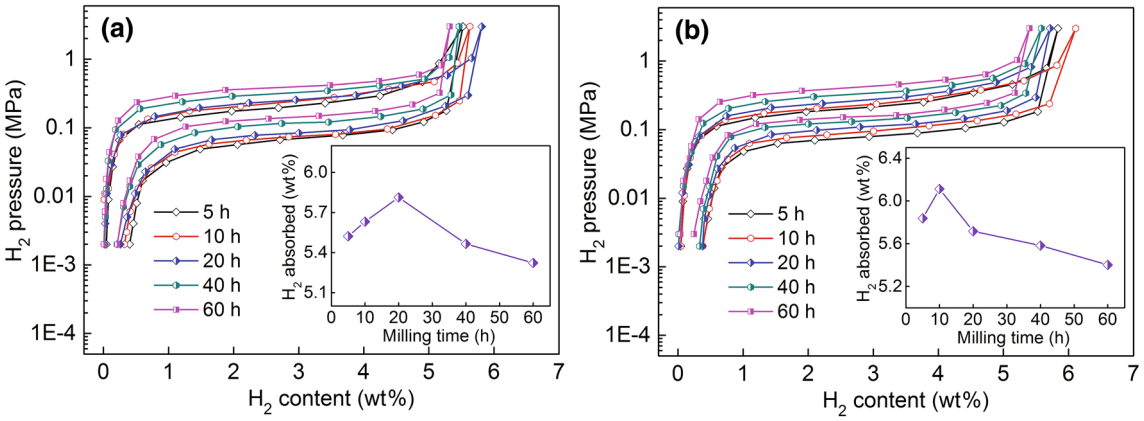

Fig. 4 *P–C–T* curves of the as-milled $NdMg_{11}Ni + x$ wt% Ni ($x = 100$, 200) alloys at 573 K. **a** $x = 100$, **b** $x = 200$

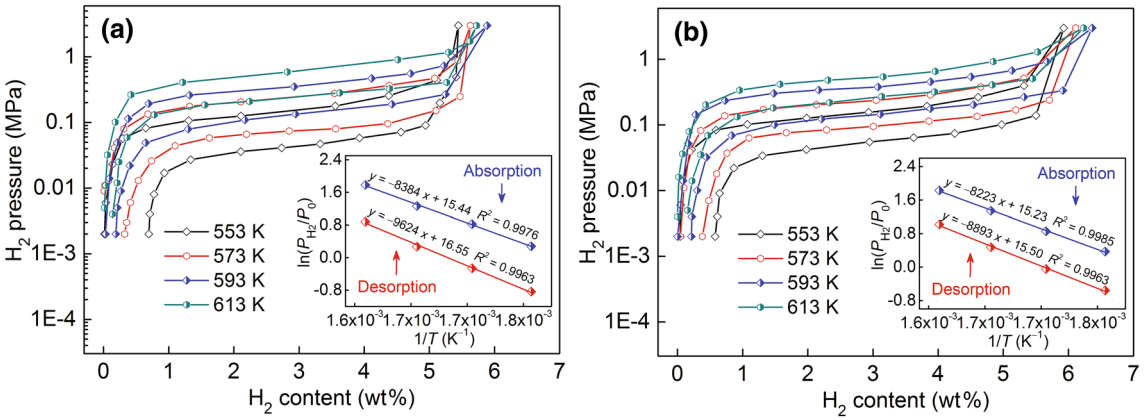

Fig. 5 *P–C–T* curves of the as-milled (10 h) $NdMg_{11}Ni + x$ wt% Ni ($x = 100$, 200) alloys in the temperature range of 553–613 K and Van't Hoff diagrams. **a** $x = 100$, **b** $x = 200$

$$\ln\left(\frac{P_{H_2}}{P_0}\right) = \frac{\Delta H}{RT} - \frac{\Delta S}{R}, \quad (1)$$

where P_{H_2} is the equilibrium hydrogen gas pressure (due to the fact that the pressure plateaus have a clear inclination, hence, we take the pressure corresponding to the 50% of the maximum hydrogen absorption/desorption capacity as equilibrium hydrogen gas pressure), P_0 is the standard atmospheric pressure, T is the sample temperature, and R is the gas constant (8.314 J/mol/K). The obtained thermodynamic parameters of the as-milled alloys are listed in Table 1. The enthalpy and entropy changes are all smaller than that of the as-cast $NdMg_{11}Ni$ alloy in our previous reports ($\Delta H_a = -79$ kJ/mol H_2, $\Delta S_a = -134$ J/K/mol H_2 for absorption, and $\Delta H_d = -83$ kJ/mol H_2, $\Delta S_d = -139$ J/K/mol H_2 for desorption) [24]. In addition, increasing Ni content from 100 to 200 brings on a slight decrease in the thermodynamic properties of the as-milled alloys.

3.3 Hydrogen Absorption and Desorption Kinetics

To investigate the hydrogen absorption kinetics, the hydrogen absorption capacities of the as-milled $NdMg_{11}Ni + x$ wt% Ni ($x = 100$, 200) alloys as functions

Table 1 Enthalpy and entropy changes of the as-milled alloys

$NdMg_{11}Ni + x$ wt% Ni	Absorption		Desorption	
	ΔH (kJ/mol H_2)	ΔS (J/K/mol H_2)	ΔH (kJ/mol H_2)	ΔS (J/K/mol H_2)
$x = 100$	−69	−128	80	137
$x = 200$	−68	−126	74	129

of reaction time are measured at 573 K and 3 MPa, as depicted in Fig. 6. The as-milled alloys exhibit a very fast hydrogen absorption rate in the initial stage, and after that the hydrogen content is almost saturated at the next quite a long hydrogenation time. Just as the hydrogen absorption capacity, the hydrogen absorption rate is also extremely important for hydrogen storage materials applied in an onboard hydrogen storage system. Here, the hydriding kinetics of hydrogen storage alloys is symbolized by hydrogen absorption saturation ratio (R_t^{a}). This parameter is the ratio of the hydrogen absorption capacity at a fixed time to the saturated hydrogen absorption capacity of an alloy. It can be defined as $R_t^{\mathrm{a}} = C_t^{\mathrm{a}}/C_{100}^{\mathrm{a}} \times 100(\%)$, where C_t^{a} and C_{100}^{a} are the hydrogen absorption capacities at t min and 100 min, respectively. In the experiment, we found that the C_{100}^{a} values of all the experimental alloys are more than 98% of their saturated hydrogen absorption capacity. Therefore, the C_{100}^{a} value can be reasonably considered as the saturated hydrogen absorption capacity of the alloys. For a better comparison, taking hydrogen absorption time of 10 min as a benchmark, thus the relationship between the R_{10}^{a} ($t = 10$) values of the as-milled alloys and milling time is established (inset in Fig. 6). It is obvious that the R_{10}^{a} values of the as-milled alloys first increase and then decrease with prolonging milling time, and the maximum R_{10}^{a} values of the as-milled $NdMg_{11}Ni + x$ wt% Ni ($x = 100$, 200) are 89.1 and 99.6%, respectively. We also note that the ($x = 200$) alloy exhibits a much higher R_{10}^{a} value at the same milling time, indicating that the increase in Ni content generates relatively catalytic alloy surface for the hydrogen reactions in the process of ball milling. The enhanced H_2 absorption kinetics caused by increasing Ni content may be ascribed to the increases in both grain and phase boundaries. Wang et al. [25] reported that the contribution of the grain boundary to hydrogen transportation was represented by the differences of diffusivity (and permeability) in single crystal nickel and directionally solidified nickel. Similarly, the hydrogen desorption kinetics of an alloy is characterized by hydrogen desorption ratio (R_t^{d}), a ratio of the hydrogen desorption capacity at a fixed time to the saturated hydrogen absorption capacity, which is defined as $R_t^{\mathrm{d}} = C_{\mathrm{t}}^{\mathrm{d}}/C_{100}^{\mathrm{a}} \times 100(\%)$, where C_{100}^{a} is the same as the previous definition and C_t^{d} is the hydrogen desorption capacity at t min. For facilitating comparison, hydrogen absorption time of 20 min is taken as a measure to establish the relationship between the R_{20}^{d} values of the as-milled alloys and milling time, as illustrated in Fig. 7. It can be observed that the dehydrogenation rates of the alloys clearly increase with prolonging milling time. More specifically, extending milling time from 5 to 60 h results in the R_{20}^{d} value rising from 23.2% to 29.9% for the $x = 100$ alloy and from 25.8% to 35.5% for the $x = 200$ alloy, respectively.

Figure 8 presents the variations of the hydrogen desorption capacities of the as-milled (10 h) $NdMg_{11}Ni + x$ wt% Ni ($x = 100$, 200) alloys in the temperature range from 553 to 613 K with reaction time. It is observed that the hydrogen desorption kinetics is very intensive to reaction temperature. In addition, it is found that the $x = 200$ alloy displays faster dehydriding kinetics than $x = 100$ alloy for all the dehydriding temperatures, meaning that increasing Ni content facilitates the improvement in the dehydriding kinetics of the alloys.

3.4 Hydrogen Desorption Activation Energy

The gas–solid reaction kinetics is generally considered to depend on its activation energy, which represents the total potential barrier what a gas–solid reaction must overcome. As for gaseous hydrogen desorption reaction, it is usually believed to be associated with total energy barrier

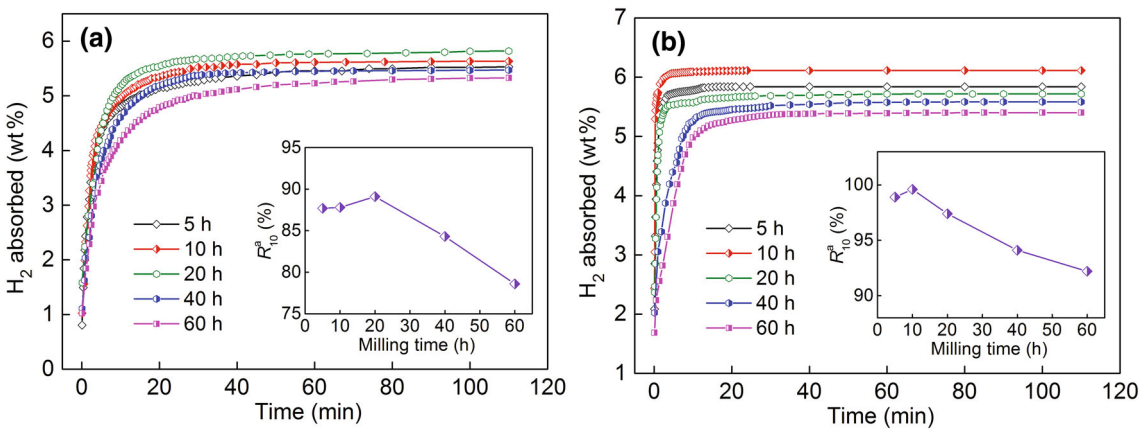

Fig. 6 Hydrogen absorption kinetic curves of the as-milled $NdMg_{11}Ni + x$ wt% Ni ($x = 100$, 200) alloys at 573 K. **a** $x = 100$, **b** $x = 200$

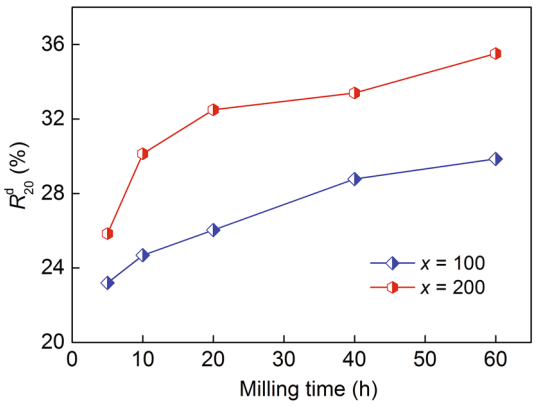

Fig. 7 Evolutions of the R^d_{20} values of the as-milled $NdMg_{11}Ni + x$ wt% Ni ($x = 100$, 200) alloys at 573 K alloys with milling time

concerning hydrogen desorption processes [26]. Hence, the activation energy has been widely used to evaluate the driving force of hydrogen desorption reaction. In this work, we use two methods, Arrhenius and Kissinger methods, to calculate the hydrogen desorption activation energy of the alloys. Firstly, Arrhenius and Johnson–Mehl–Avrami (JMA) equations are used to determine the dehydrogenation activation energy (E^{de}_a). Arrhenius equation [27] is as follows:

$$k = A\exp\left(\frac{-E^{de}_a}{RT}\right), \tag{2}$$

where A is a temperature-independent coefficient, R is the universal gas constant (8.314 J/mol/K), T is the absolute temperature, and k is an effective kinetic parameter. The hydrogen desorption curves have been analyzed by using JMA equation [28, 29]:

$$\ln[-\ln(1-\alpha)] = \eta \ln k + \eta \ln t, \tag{3}$$

where α is the phase fraction transformed at time t which can be identified with a normalized hydrogen weight percentage (from 0 to 1), and η is the Avrami exponent. Based on the data in Fig. 8, we can use logarithmic transform of Eq. (3) to construct a graph of $\ln[-\ln(1-\alpha)]$ versus $\ln t$ at 553, 573, 593 and 613 K, respectively, which is termed as Avrami plot as shown in Fig. 9. It is found that the Avrami plots are nearly linear; hence, we can derive $\ln k$ values from the intercepts of the Avrami plots of $\ln[-\ln(1-\alpha)]$ versus $\ln t$. Further linear fitting can be done by plotting $\ln k$ versus $1/T$, which is termed as Arrhenius plot as the inset in Fig. 9. Thus, the E^{de}_a can be easily calculated from the slope of the Arrhenius plot. The E^{de}_a value of the as-milled (10 h) $NdMg_{11}Ni + x$ wt% Ni ($x = 100$, 200) alloys is 82 and 69 kJ/mol, respectively. It is very evident that increasing Ni content gives rise to a clear decrease in the hydrogen desorption activation energy of the as-milled alloy. Ouyang et al. [30] also reported that E_a values can be determined as 63 ± 3 kJ/mol H_2 for $CeH_{2.73}$–MgH_2–Ni composites and 104 ± 7 kJ/mol H_2 for $CeH_{2.73}$–MgH_2, respectively. This is mainly because of catalyst effects of $CeH_{2.73}$ and Mg_2NiH_4.

At present, we use Kissinger method to calculate the hydrogen desorption activation energy. Kissinger equation is as follows [31]:

$$\frac{d\left[\ln\left(\beta/T^2_p\right)\right]}{d\left(1/T_p\right)} = \frac{-E^{de}_k}{R}, \tag{4}$$

where E^{de}_k is activation energy, β is the heating rate, T_p is the absolute temperature corresponding to the maximum desorption rate in the DSC curves, and R is the universal gas constant (8.314 J/mol/K). In consideration of the calculation conditions of Kissinger method, the hydrogen desorption reactions of the as-milled (10 h)

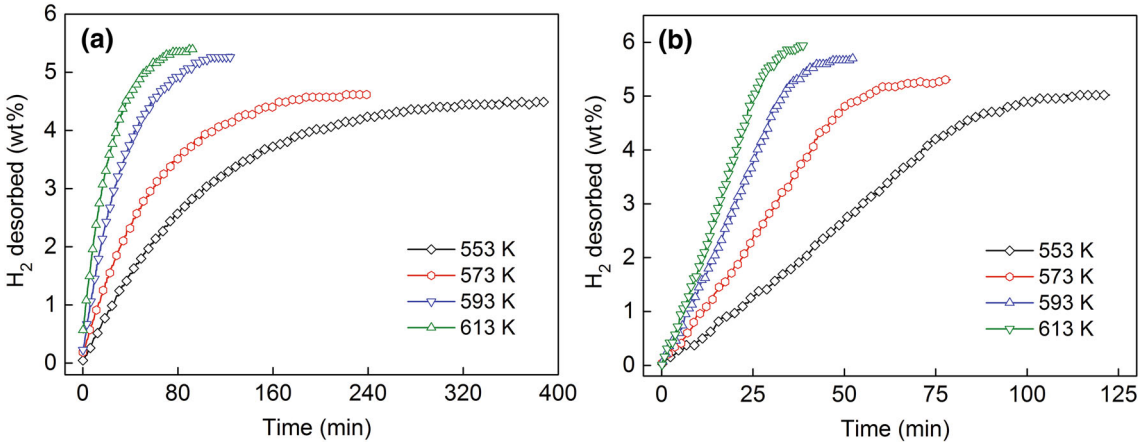

Fig. 8 Hydrogen desorption kinetic curves of the as-milled (10 h) $NdMg_{11}Ni + x$ wt% Ni ($x = 100$, 200) alloys at 553, 573, 593 and 613 K. **a** $x = 100$, **b** $x = 200$

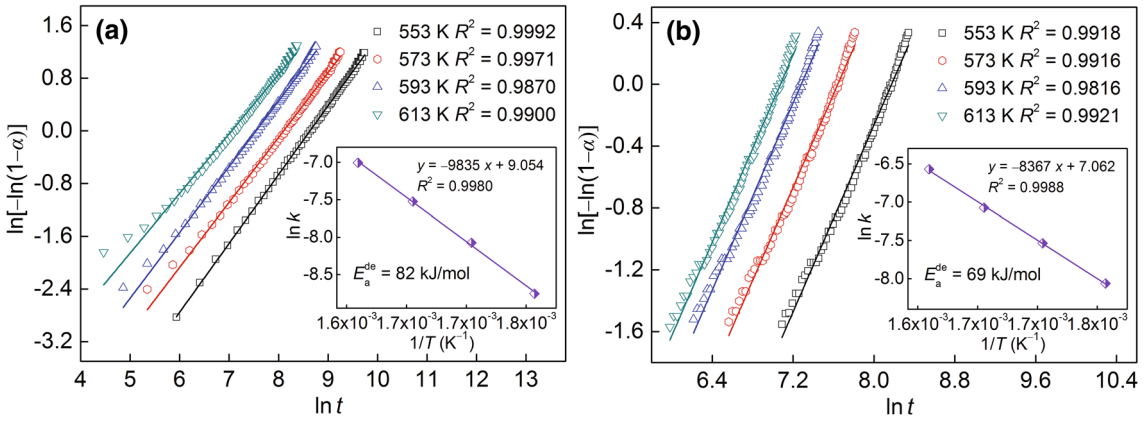

Fig. 9 Plots of ln[–ln(1–α)] versus ln t of the as-milled (10 h) $NdMg_{11}Ni + x$ wt% Ni (x = 100, 200) alloys at 553, 573, 593 and 613 K and Arrhenius plots. **a** x = 100, **b** x = 200

$NdMg_{11}Ni + x$ wt% Ni (x = 100, 200) alloys in the saturated hydrogen absorbing state at 573 K and 3 MPa are measured by DSC at the heating rates of 5, 10, 15 and 20 K/min, respectively, as depicted in Fig. 10. Clear endothermic peaks, which correspond to the hydrogen desorption, are observed. All alloys display similar peak shapes, suggesting that each reaction involves in the same reaction process. Meanwhile, the endothermic peak of the x = 200 alloy has a drift to low temperatures for each heating rate, meaning that the reaction rate can be improved by increasing Ni content in the process of desorption hydrogen as well. On the basis of the data in Fig. 10, we can use logarithmic transformation of Eq. (4) to construct a graph of $\ln(\beta/T_p^2)$ versus $1/T_p$, namely Kissinger plots as shown in the inset of Fig. 10, which are found to be nearly linear. Thereby, we can easily calculate the activation energy E_k^{de} from the slope of the Kissinger plot. The E_k^{de} values of the as-milled (10 h) $NdMg_{11}Ni + x$ wt% Ni (x = 100, 200) alloys are 73 and 64 kJ/mol, respectively.

To compare the difference in the hydrogen desorption activation energies calculated by two methods, we calculate the hydrogen desorption activation energies of the as-milled $NdMg_{11}Ni + x$ wt% Ni (x = 100, 200) alloys using the two methods and establish the relationships between the E^{de} (for Arrhenius method $E^{de} = E_a^{de}$; for Kissinger method $E^{de} = E_k^{de}$) values of the alloys and milling time, as illustrated in Fig. 11. It is observed that the E^{de} values of the alloys decrease with prolonging milling time. So, we can infer that the hydrogen desorption kinetics ameliorated by extending milling time is ascribed to the decrease in the activation energy. In addition, increasing Ni content results in a decrease in the hydrogen desorption activation energy, regardless of the method used. This characteristic is inferred to be the root cause of the amelioration of the hydrogen desorption kinetics of the alloys facilitated by

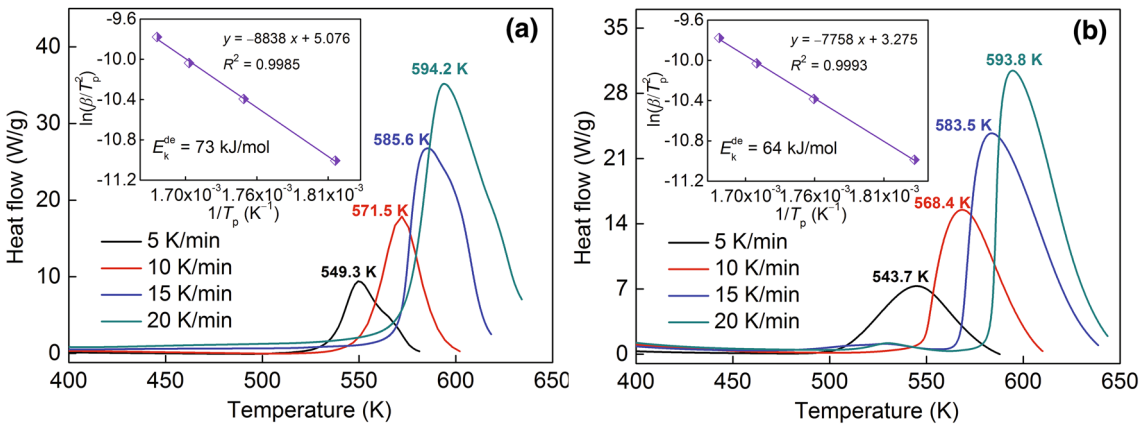

Fig. 10 DSC curves of the as-milled (10 h) $NdMg_{11}Ni + x$ wt% Ni (x = 100, 200) alloys at various heating rates and Kissinger plots. **a** x = 100, **b** x = 200

increasing Ni content. Furthermore, we also find that the activation energy calculated by Arrhenius method is larger than that by Kissinger method. A very similar result was reported by Baricco et al. [32].

As far as the above-mentioned results are concerned, some elucidations can be provided for the effects of Ni content and milling time on the hydrogen absorption and desorption kinetics of the alloys. In respect of the positive contribution of the mechanical milling to the hydrogen storage kinetics, it is convinced to be associated with the changed structure of the alloy generated by ball milling. After being mechanically milled, the crystalline alloy becomes at least partially disordered and its structure changes into nanocrystalline or amorphous. Meanwhile, a lot of new crystallites and grain boundaries occur, which can provide numerous sites with low diffusion activation energy, thus facilitating the diffusion of hydrogen atoms in alloys [33]. Moreover, it is noteworthy that the ball milling for a longer time (more than 20 h for the $x = 100$ alloy or 10 h for the $x = 200$ alloy) will induce an undesirable decrease in the hydriding rate of the alloys, which is ascribed to the facilitated glass forming by adding Ni due to the fact that the diffusion ability of hydrogen atoms in an amorphous phase is much lower than that in a nanocrystalline phase. With regard to the positive action of increasing milling time on the hydrogen desorption kinetics, it is now well established that reducing grain size far below the micrometer scale can dramatically improve the dehydrogenation properties of Mg-based alloys [9, 34]. The improved hydrogen absorption and desorption kinetics by increasing Ni content are believed to create high catalytic alloy surface for the hydrogen reactions during mechanical milling [35].

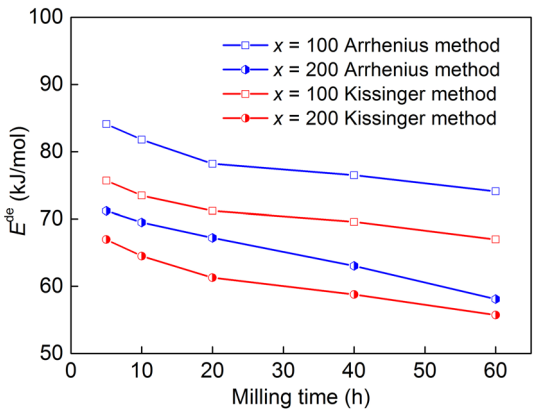

Fig. 11 Variations of hydrogen desorption activation energies of the as-milled $NdMg_{11}Ni + x$ wt% Ni ($x = 100, 200$) alloys calculated by Arrhenius and Kissinger methods with milling time

4 Conclusions

1. Increasing Ni content brings on a slight decrease in the thermodynamic parameters (ΔH and ΔS) of the as-milled alloys and dramatically improves the hydrogen absorption and desorption kinetics properties of the alloys.
2. The gaseous hydrogen absorption capacity (C^{a}_{100}) and kinetics (R^{a}_{10}) of the alloys reach the maximum values with varying milling time. However, the hydrogen desorption kinetics (R^{d}_{20}) always increases with prolonging milling time.
3. Arrhenius and Kissinger methods have been used to evaluate the hydrogen desorption activation energy of the as-milled alloy. The results both indicate that the hydrogen desorption activation energy of the alloys obviously decrease with increasing Ni content and prolonging milling time. This characteristic is the real driving force of the improved hydrogen desorption kinetics of the as-milled alloys caused by increasing Ni content and prolonging milling time.

Acknowledgments This work is financially supported by the National Natural Science Foundation of China (Nos. 51371094 and 51471054).

References

[1] H. Wang, A.K. Prasad, S.G. Advani, Int. J. Hydrog. Energy **37**, 290 (2012)
[2] L. Schlapbach, A. Züttel, Nature **414**, 353 (2001)
[3] L.Z. Ouyang, J.J. Tang, Y.J. Zhao, H. Wang, X.D. Yao, J.W. Liu, J. Zou, M. Zhu, Sci. Rep. **5**, 10776 (2015)
[4] Y.H. Zhang, Z.M. Yuan, T. Yang, Z.H. Hou, D.L. Zhao, Acta Metall. Sin. (Engl. Lett.) **28**, 826 (2015)
[5] K. O'Malley, G. Ordaz, J. Adams, K. Randolph, C.C. Ahn, N.T. Stetson, J. Alloys Compd. **645**, S419 (2015)
[6] T. Umegaki, J.M. Yan, X.B. Zhang, H. Shioyama, N. Kuriyama, Q. Xu, Int. J. Hydrog. Energy **34**, 2303 (2009)
[7] Y. Wang, W.Q. Deng, X.W. Liu, S.Y. Wang, X. Wang, Int. J. Hydrog. Energy **34**, 1444 (2009)
[8] Y. Wang, S.Z. Qiao, X. Wang, Int. J. Hydrog. Energy **33**, 5066 (2008)
[9] S. Kalinichenka, L. Röntzsch, T. Riedl, T. Gemming, T. Weißgärber, B. Kieback, Int. J. Hydrog. Energy **36**, 1592 (2011)
[10] L.Z. Ouyang, F.X. Qin, M. Zhu, Scr. Mater. **55**, 1075 (2006)
[11] L.Z. Ouyang, X.S. Yang, H.W. Dong, M. Zhu, Scr. Mater. **61**, 339 (2009)
[12] H.W. Dong, L.Z. Ouyang, T. Sun, M. Zhu, J. Rare Earth **26**, 303 (2008)
[13] M. Hossein Enayati, F. Karimzadeh, S. Sabooni, M. Jafari, Acta Metall. Sin. (Engl. Lett.) **28**, 1002 (2015)
[14] T. Spassov, V. Rangelova, N. Neykov, J. Alloys Compd. **334**, 219 (2002)
[15] H. Gu, Y. Zhu, L. Li, Int. J. Hydrog. Energy **33**, 2970 (2008)
[16] A.M. Jorge, E. Prokofiev, G.F. de Lima, E. Rauch, M. Veron, W.J. Botta, M. Kawasaki, T.G. Langdon, Int. J. Hydrog. Energy **38**, 8306 (2013)

[17] Y. Wang, X. Wang, C.M. Li, Int. J. Hydrog. Energy **35**, 3550 (2010)
[18] A.A. Poletaev, R.V. Denys, J.P. Maehlen, J.K. Solberg, B.P. Tarasov, V.A. Yartys, Int. J. Hydrog. Energy **37**, 3548 (2012)
[19] Q.A. Zhang, C.J. Jiang, D.D. Liu, Int. J. Hydrog. Energy **37**, 10709 (2012)
[20] M. Abdellaoui, S. Mokbli, F. Cuevas, M. Latroche, A. Percheron-Guégan, H. Zarrouk, J. Alloys Compd. **356–357**, 557 (2003)
[21] R.V. Denys, A.A. Poletaev, J.K. Solberg, B.P. Tarasov, V.A. Yartys, Acta Mater. **58**, 2510 (2010)
[22] R.V. Denys, A.A. Poletaev, J.P. Maehlen, J.K. Solberg, B.P. Tarasov, V.A. Yartys, Int. J. Hydrog. Energy **37**, 5710 (2012)
[23] H. Falahati, D.P.J. Barz, Int. J. Hydrog. Energy **38**, 8838 (2013)
[24] Y.H. Zhang, Z.C. Jia, Z.M. Yuan, Y. Qi, Z.H. Hou, D.L. Zhao, Int. J. Mater. Res. (2016). doi:10.3139/146.111345
[25] Y.L. Wang, L.Y. Xiong, S.R. Liu, Acta Metall. Sin. (Engl. Lett.) **27**, 615 (2014)
[26] T. Sadhasivam, M.S.L. Hudson, S.K. Pandey, A. Bhatnagar, M.K. Singh, K. Gurunathan, O.N. Srivastava, Int. J. Hydrog. Energy **38**, 7353 (2013)
[27] K.J. Laidler, Pure Appl. Chem. **68**, 149 (1996)
[28] T. Yang, Z.M. Yuan, W.G. Bu, Z.C. Jia, Y. Qi, Y.H. Zhang, Int. J. Hydrog. Energy **41**, 2689 (2016)
[29] J.F. Fernandez, C.R. Sanchez, J. Alloys Compd. **356–357**, 348 (2003)
[30]. L.Z. Ouyang, X.S. Yang, M. Zhu, J.W. Liu, H.W. Dong, D.L. Sun, J. Zou, X.D. Yao, J. Phys. Chem. C **118**, 7808 (2014)
[31] H.E. Kissinger, Anal. Chem. **29**, 1702 (1957)
[32] M. Baricco, M.W. Rahman, S. Livraghi, A. Castellero, S. Enzo, E. Giamello, J. Alloys Compd. **536**, S216 (2012)
[33] Y. Wu, W. Han, S.X. Zhou, M.V. Lototsky, J.K. Solberg, V.A. Yartys, J. Alloys Compd. **466**, 176 (2008)
[34] M.Y. Song, C.D. Yim, S.N. Kwon, J.S. Bae, S.H. Hong, Int. J. Hydrog. Energy **33**, 87 (2008)
[35] M. Anik, J. Alloys Compd. **491**, 565 (2010)